Journal of Advanced Research 32 (2021) 45–60

Contents lists available at ScienceDirect

Journal of Advanced Research

journal homepage: www.elsevier.com/locate/jare

A local stabilized approach for approximating the modified time-fractional diffusion problem arising in heat and mass transfer

O. Nikan [a], Z. Avazzadeh [b,*], J.A. Tenreiro Machado [c]

[a] School of Mathematics, Iran University of Science and Technology, Narmak, Tehran, Iran
[b] Department of Applied Mathematics, Xi'an Jiaotong-Liverpool University, Suzhou 215123, China
[c] Institute of Engineering, Polytechnic of Porto, Department of Electrical Engineering, Rua Dr. António Bernardino de Almeida, 431, 4249-015 Porto, Portugal

HIGHLIGHTS

- The modified time-fractional diffusion model plays an important role in heat transfer and fluid flow problems.
- A meshless method based on hybridization of Gaussian and cubic kernels is developed to solve the model.
- The proposed method has good accuracy and applicable over complex domains with various node distributions.
- The time-discrete algorithm is examined in terms of the convergence and unconditional stability properties using the energy method.

GRAPHICAL ABSTRACT

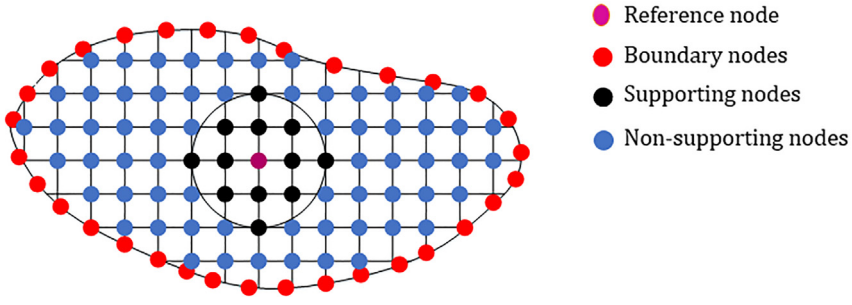

ARTICLE INFO

Article history:
Received 16 September 2020
Revised 11 December 2020
Accepted 4 March 2021
Available online 10 March 2021

2010 MSC:
35R11
65M06
65M12

Keywords:
Modified time fractional diffusion problem
Local hybrid kernel meshless method
Finite difference
RBF-FD
Convergence and Stability

ABSTRACT

Introduction: During the last years the modeling of dynamical phenomena has been advanced by including concepts borrowed from fractional order differential equations. The diffusion process plays an important role not only in heat transfer and fluid flow problems, but also in the modelling of pattern formation that arises in porous media. The modified time-fractional diffusion equation provides a deeper understanding of several dynamic phenomena.
Objectives: The purpose of the paper is to develop an efficient meshless technique for approximating the modified time-fractional diffusion problem formulated in the Riemann–Liouville sense.
Methods: The temporal discretization is performed by integrating both sides of the modified time-fractional diffusion model. The unconditional stability of the time discretization scheme and the optimal convergence rate are obtained. Then, the spatial derivatives are discretized through a local hybridization of the cubic and Gaussian radial basis function. This hybrid kernel improves the condition of the system matrix. Therefore, the solution of the linear system can be obtained using direct solvers that reduce significantly computational cost. The main idea of the method is to consider the distribution of data points over the local support domain where the number of points is almost constant.
Results: Three examples show that the numerical procedure has good accuracy and applicable over complex domains with various node distributions. Numerical results on regular and irregular domains illustrate the accuracy, efficiency and validity of the technique.

☆ Peer review under responsibility of Cairo University.

* Corresponding author.
E-mail addresses: omidnikan77@yahoo.com (O. Nikan), zakieh.avazzadeh@xjtlu.edu.cn (Z. Avazzadeh), jtm@isep.ipp.pt (J.A.T. Machado).

https://doi.org/10.1016/j.jare.2021.03.002

Conclusion: This paper adopts a local hybrid kernel meshless approach to solve the modified time-fractional diffusion problem. The main results of the research is the numerical technique with non-uniform distribution in irregular grids.

Introduction

During the last years the modeling of dynamical phenomena has been advanced by including concepts borrowed from fractional order differential equations (FDEs). This generalisation of derivatives and integrals led to the field of mathematics called fractional calculus [1,2]. The history of fractional calculus started in the 17th century, but only recently became popular in applied sciences. The application of FDEs has expanded rapidly and we can mention for example the analysis of problems such as creep or relaxation in visco-elastoplastic materials, diffusion process models, control, and plasma physics problems [3–6]. Nonetheless, in many applications is necessary to solve FDEs using efficient numerical techniques [7–14].

The diffusion process plays an important role not only in heat transfer and fluid flow problems, but also in the modelling of pattern formation that arise in porous media. The time-fractional diffusion equation describes the mass transfer processes involving memory effects [15]. The mean square displacement (MSD) of the diffusing species in standard diffusion is linear with respect to time. One can define the MSD as a product of the diffusion coefficient and time [16].

If the memory effects are present to some mass transfer, then the process no longer follows a Brownian motion and the diffusion species cannot be described by the Fick's second law [17]. In these cases, the time-fractional diffusion equation can explain better the dynamic phenomena. Indeed, various types of complex transport processes can be described by means of the fractional order derivative, so that $\langle x^2(t)\rangle \sim K_\gamma t^\gamma$, where x, t and $K_\gamma \geqslant 0$ denote the displacement, time and generalized diffusion coefficient. Otherwise, if $0 < \gamma < 1$, then the sub-diffusive transport regime holds, meaning that it has a smaller speed than the normal diffusion. If the fractional order lies in the range $1 < \gamma < 2$, then the super-diffusive transport regime holds and exhibits a larger speed than the classical Fickian transport [18,19]. These models commonly occur within media with porous or fractal structures [20]. Unlike the classical case, the anomalous diffusion involves a MSD that is proportional to the power of time with non-integer order. For describing the statistical probability of the position of a particle is the continuous time random walk (CTRW) model is often employed, which is related to the Lévy diffusion process [21–24].

The anomalous diffusion and its corresponding regime may have different physical roots depending on each particular case [25]. Nonetheless, this dynamical phenomenon is different from the traditional Knudsen and Fickian diffusion, where the physical roots are clear. The two types of diffusion are governed by a Markovian type Wiener Brownian motion, and the corresponding pores have a smaller size than the species mean free path. In viscoelastic media it is the additional degree of freedom that drives the sub-diffusive regime, while in chaotic systems, the presence of traps that cause the anomalous diffusion [25]. Non-usual diffusion can be also created as a result of the fractal structure in solid media [20]. If the inertial forces of the particles dominate over the inter-particle frictional forces, then we can obtain a deviation from the standard Fickian transport [26]. Mass transfer kinetics in the scope of the gaseous transport within restricted porous media is described by the retention time of the diffusing species in the pores of the solid media.

The retention time can be related to geometrical confinements within the pores and the diffusing species adsorption on the surface inside the pores. As a result of the adsorption process, the diffusing molecules remain at a particular location for different time intervals. This behaviour can be due to the energy disorder on the surface of the porous solid media. The time delays control the memory effects and the nonlinearity of the random movement of particles, leading to a non-Markov Brownian motion described by the CTRW model. As a result, the fractional derivative replaces the temporal derivative of integer order in the transport equation with much better modelling results [27].

We study numerical solution for the modified time-fractional diffusion equation (MTFDE) including two time fractional derivatives

$$\frac{\partial u(\mathbf{x},t)}{\partial t} - v_1 \mathrm{D}_t^{1-\alpha}\Delta u(\mathbf{x},t) - v_2 \mathrm{D}_t^{1-\beta}\Delta u(\mathbf{x},t) = f(\mathbf{x},t), \quad \mathbf{x} \in \Omega, \quad 0 < t \leqslant T, \tag{1}$$

with the following initial and boundary conditions:

$$u(\mathbf{x},0) = h(\mathbf{x}), \qquad \mathbf{x} \in \Omega, \tag{2}$$

$$u(\mathbf{x},t) = g(\mathbf{x},t), \qquad t > 0, \ \mathbf{x} \in \partial\Omega, \tag{3}$$

where the constants v_1 and v_2 are positive, $\mathbf{x} = (x, y)$ stands for the space variable, $\partial\Omega$ is the closed contour bounding the region, $0 < \alpha, \beta < 1, \overline{\Omega} = \Omega \cup \partial\Omega \subset \mathbb{R}^2$ represents the spatial domain, and $\Delta$is the Laplacian operator with respect to the spatial variables. Additionally, $f(\mathbf{x}, t)$ is the forcing term with satisfactory smoothness and $h(\mathbf{x})$ is a given continuous function. The fractional diffusion terms $\mathrm{D}_t^{1-\alpha}\Delta u(\mathbf{x}, t)$ and $\mathrm{D}_t^{1-\beta}\Delta u(\mathbf{x}, t)$ reflect the anomalous subdiffusion behavior of diffusion processes. The fractional operator $\mathrm{D}_t^{1-\gamma} z(\mathbf{x}, t)$ represents the Riemann–Liouville (R-L) fractional derivative with respect to time variable t, formulated as

$$\mathrm{D}_t^{1-\gamma} z(\mathbf{x},t) = \frac{1}{\Gamma(\gamma)} \frac{\partial}{\partial t} \int_0^t \frac{z(\mathbf{x},s)}{(t-s)^{1-\gamma}} \mathrm{d}s,$$

where $\Gamma(\cdot)$ is Gamma function.

This model has been applied in econophysics due to the an increasing interest in describing CTRW-like effects [28]. Some numerical approaches have been presented for solving MTFDE. Liu et al. [29] and Mohebbi et al. [30] developed the finite element and the RBF meshless methods, respectively. Dehghan et al. [31] and Wang et al. [32] formulated the Legendre spectral element and the compact locally finite difference techniques, respectively. Li and Wang [33] proposed a compact difference algorithm to approximate the MTFDE. Shivanian and Jafarabadi [34] presented a radial point interpolation, while Cao et al. [35] adopted an implicit midpoint scheme for approximating MTFDE.

A crucial issue when analysing complex scientific processes is the numerical modeling and simulation. Such processes are usually obtained both at large or small scales, and pose difficulties for an interpretation using direct measurements. Important developments in numerical techniques include the finite volume (FV), finite element (FE), finite difference (FD), and pseudo-spectral (PS) approaches. These techniques provide an approximate solution to the governing equations over a distribution of elements, or nodes, structured in a point grid or mesh. A set of meshless numerical techniques emerged over the last decades. Such techniques make use of the interaction between each node and part, or all, of the surrounding nodes, by adopting a specified kernel

rather than following the connections among them. Spectral meshless techniques based on the radial basis functions (RBFs) are gaining popularity in the geosciences due to their competitive accuracy, functionality on unstructured meshes. The RBF technique is an efficient method for interpolation of multidimensional scattered data [36–38], since it does not requires meshes and is able to solve easily complex geometrical and high-dimension problems. Therefore, the RBFs became popular for approximating partial differential equations on complex domains and have been applied in the solution of physical problems with theoretical proofs on solvability and convergence [36–38].

Hardy [39] initially used the RBF to interpolate scattered points for the approximation of irregular surfaces that have an important role in meshfree techniques. Kansa [40] employed the RBF interpolation technique to obtain the approximate solution of a PDE using all the domain points (thereafter named the Kansa's method). The results obtained from applying the Kansa's method lead to a large, dense, and ill-conditioned linear system [41]. For overcoming the above problems with the Kansa's approach, a "local" version of RBF was proposed giving spectral accuracy for a sparse, better-conditioned linear system and allowing more flexibility to handle non-linearities. The RBF generated finite difference, called as RBF-FD, is another technique that is based on RBF. This method is based on generalized FD method for scattered node layouts advanced by Tolstykh [42]. The RBF-FD is a FD technique where we compute the weights by fitting an RBF interpolant to scattered nodes in one or several spatial dimensions. This strategy leads to a sparse differentiation matrix. After the differentiation matrix is created, one can use it repeatedly to approximate the spatial derivative. The RBF-FD, combining the meshless and FD methods, has attracted the attention of many scholars due to its properties. Abbaszadeh and Dehghan [43] developed a fast and efficient numerical algorithm by combining the local RBF-FD approach with the proper orthogonal decomposition (POD) and the discrete empirical interpolation method (DEIM) to simulate the time dependent incompressible Navier–Stokes model. Dehghan et al. [44] proposed a local meshless RBF-FD method for solving the regularized long-wave and extended Fisher-Kolmogorov equations in one-, two-, and three-dimensions. Dehghan and Abbaszadeh [45] considered a linear combination of the shape functions of local RBF collocation method with the moving Kriging interpolation technique. Avazzadeh et al. [46] applied the local RBF-FD to obtain the solitary wave solutions of the generalized Rosenau-Korteweg-de Vries-regularized-long wave equation. Nikan et al. [47–49] adopted the local RBF-FD collocation approach for solving the time fractional equations.

This work proposes a local stabilized approach, generated through the hybrid Gaussian-cubic RBF and FD for obtaining the solution of the MTFDE. The infinitely smooth RBF, such as Gaussian, provide an invertible system matrix in meshless methods. Nevertheless, for a large number of domain nodes and small shape parameters, a Gaussian RBF yields a system of equations that is ill-conditioned. On the other hand, the cubic RBF is infinitely smooth and without any shape parameter, unlike what occurs with the Gaussian RBF. However, using a cubic RBF to interpolate shape functions in meshless techniques for specific node arrangements has the risk of obtaining a singular system. Indeed, this paper introduces an approach to deal with these two issues through hybrid RBF combining Gaussian kernels with cubic splines. The basic idea behind such hybridization is to obtain a kernel that takes advantage of the merits of the two kernels while compensating for the limitations of each one and keeping the formulation as a standard RBF method. The outline of this paper is as follows. The Section entitled "Time-discrete formulation" accomplishes the temporal discretization by integrating both sides of the MTFDE. The stability analysis and *a priori* error estimates in H^1-norm are also discussed in detail. The Section entitled "Local hybridization of the Gaussian and cubic kernels" describes the spatial desensitization with the of the local hybrid kernel meshless techniques. The Section entitled "Numerical examples" illustrates the numerical algorithm by means of three problems that highlight the accuracy and efficiency of the proposed approach. Finally, the Section entitled "Conclusion" synthesises the main concluding remarks.

Time-discrete formulation

In this section, a time discrete algorithm to approximate the (1) in the time variable is formulated. For this purpose, we split the time interval $[0,T]$ into small cells with time step length δt and nodes $t_k = k\delta t$, for $k = 0,1,2,\ldots,M$, where M is a positive integer.

Definition 1. Suppose that $y(t) \in L^1(a,b)$, and that the expression

$$I^{\gamma}_{a^+} y(t) = \frac{1}{\Gamma(\gamma)} \int_a^t \frac{y(\eta)}{(t-\eta)^{1-\gamma}} \mathrm{d}\eta, \;\; t > a, \gamma > 0,$$

denotes the R-L fractional integral operator of order γ.

Lemma 1. ([50].) If $y(t) \in C^2[0,1]$, then

$$I^{\gamma}_{0^+} y(t_{k+1}) - I^{\gamma}_{0^+} y(t_k) = \frac{\delta t^{\gamma}}{\Gamma(\gamma+1)} \left[y(t_{k+1}) + \sum_{j=0}^{k-1} (b_j - b_{j+1}) y(t_{k-j}) \right] + R_{k,\gamma},$$

where $|R_{k,\gamma}| \leqslant C b_k \delta t^{1+\gamma}$, $1 = b_0 > b_1 > \ldots > b_k > 0$ and $b_j = (j+1)^{\gamma} - j^{\gamma}$.

Integrating both sides of Eq. (1) on $[t_k, t_{k+1}]$, gives

$$\begin{aligned} u(\mathbf{x}, t_{k+1}) - u(\mathbf{x}, t_k) = {} & \nu_1 I^{\alpha}_{0^+} \Delta u(\mathbf{x}, t_{k+1}) - \nu_1 I^{\alpha}_{0^+} \Delta u(\mathbf{x}, t_k) \\ & + \nu_2 I^{\beta}_{0^+} \Delta u(\mathbf{x}, t_{k+1}) - \nu_2 I^{\beta}_{0^+} \Delta u(\mathbf{x}, t_k) \\ & + \int_{t_k}^{t_{k+1}} f(\mathbf{x}, \eta) \mathrm{d}\eta. \end{aligned} \tag{4}$$

By means of Lemma 1 and the following equation

$$\int_{t_k}^{t_{k+1}} f(\mathbf{x}, \eta) \mathrm{d}\eta = \delta t f(\mathbf{x}, t_{k+1}) + O(\delta t^2),$$

we obtain

$$\begin{aligned} u^{k+1} - (\mu_1 + \mu_2) \Delta u^{k+1} = {} & u^k + \mu_1 \sum_{j=0}^{k-1} (\lambda_{j+1} - \lambda_j) \Delta u^{k-j} \\ & + \mu_2 \sum_{j=0}^{k-1} (\omega_{j+1} - \omega_j) \Delta u^{k-j} \\ & + \delta t f^{k+1} + \delta t R^{k+1}, \end{aligned} \tag{5}$$

where $\mu_1 = \frac{\nu_1 \delta t^{\alpha}}{\Gamma(1+\alpha)}$, $\mu_2 = \frac{\nu_2 \delta t^{\beta}}{\Gamma(1+\beta)}$, $\lambda_j = (j+1)^{\alpha} - j^{\alpha}$, $\omega_j = (j+1)^{\beta} - j^{\beta}$ and $R^{k+1} = \mathcal{O}\left(\delta t^{1+\min\{\alpha,\beta\}}\right)$.

By eliminating the small error term R^{k+1} and introducing U^{k+1} as the numerical approximation, results:

$$\begin{aligned} & U^{k+1} - (\mu_1 + \mu_2) \Delta U^{k+1} \\ & = U^k + \mu_1 \sum_{j=0}^{k-1} (\lambda_{j+1} - \lambda_j) \Delta U^{k-j} + \mu_2 \sum_{j=0}^{k-1} (\omega_{j+1} - \omega_j) \Delta U^{k-j} + \delta t f^{k+1}. \end{aligned} \tag{6}$$

Theoretical analysis of the difference scheme

We define the functional spaces endowed with the standard norms and inner products for the proposed difference algorithm as

$$H^1(\Omega)=\left\{v\in L^2(\Omega),\frac{\mathrm{d}v}{\mathrm{d}x}\in L^2(\Omega)\right\},$$

$$H_0^1(\Omega)=\left\{v\in H^1(\Omega),v|_{\partial\Omega}=0\right\},$$

$$H^m(\Omega)=\left\{v\in L^2(\Omega),\ \mathrm{D}^\alpha v\in L^2(\Omega)\mathrm{forallpositiveinteger}|\alpha|\leqslant m\right\},$$

where $\Omega\subset\mathbb{R}^d$ denotes bounded and open domain, $\alpha=(\alpha_1,\ldots,\alpha_d)$ represents a d-tuple, and $|\alpha|=\sum_{i=1}^d\alpha_i$, with $\mathrm{D}^\alpha v=\frac{\partial^{|\alpha|}v}{\partial x_1^{\alpha}\partial x_2^{\alpha}\ldots\partial x_d^{\alpha}}$, and $H^m(\Omega)$ is a Hilbert space with the inner product

$$\langle u,v\rangle_m=\sum_{|\alpha|\leqslant m}\int_\Omega \mathrm{D}^\alpha u(x)\mathrm{D}^\alpha v(x)\mathrm{d}x,$$

and associated norm

$$\|u\|_{H^m(\Omega)}=\left(\sum_{|\alpha|\leqslant m}\|\mathrm{D}^\alpha u\|^2_{L^2(\Omega)}\right)^{\frac{1}{2}}.$$

Nonetheless, instead of adopting the above standard H^1-norm, we define $\|\cdot\|_{H^1(\Omega)}$ by

$$\|v\|_{H^1(\Omega)}=\left[\|v\|^2+\mu_1\|\nabla v\|^2+\mu_2\|\nabla v\|^2\right]^{1/2},$$

where μ_1 and μ_2 are constant.

The error analysis of the proposed algorithm (6) follows the ideas discussed in [31,30]. For this, we start with the following definition and lemma.

Definition 2. ([51]) A finite difference algorithm is called to be stable for the norm $\|\cdot\|$, if we have two constants $C_1>0$ and $C_2>0$, independent of δt, such that when δt approaches zero, we can write:

$$\left\|V^k\right\|\leqslant C_1\left\|V^0\right\|+C_2\|f\|,\tag{7}$$

where f and V^0 represent the source term and the initial data, respectively.

Lemma 2. ([52]). If we consider

$$\eta_{k+1}=\frac{\delta t^\alpha}{\Gamma(\alpha)(k+1)^{1-\alpha}},\qquad \xi_{k+1}=\frac{\delta t^\beta}{\Gamma(\beta)(k+1)^{1-\beta}},$$

then we have the following inequalities:

$$\mu_1\lambda_{k+1}\leqslant\eta_{k+1}\leqslant\mu_1\lambda_k,\qquad \mu_2\omega_{k+1}\leqslant\xi_{k+1}\leqslant\mu_2\omega_k.$$

Theorem 1. If $U^k\in H_0^1(\Omega)$, then the implicit numerical method (6) is un-conditionally stable in the H^1-norm.

Proof. We multiply Eq. (6) by U^{k+1} and integrate on Ω,

$$\begin{aligned}&\|U^{k+1}\|^2+\mu_1\|\nabla U^{k+1}\|^2+\mu_2\|\nabla U^{k+1}\|^2\\&=\left\langle U^k,U^{k+1}\right\rangle+\mu_1\sum_{j=0}^{k-1}(\lambda_{j+1}-\lambda_j)\left\langle\nabla U^{k-j},\nabla U^{k+1}\right\rangle\\&\quad+\mu_2\sum_{j=0}^{k-1}(\omega_{j+1}-\omega_j)\left\langle\nabla U^{k-j},\nabla U^{k+1}\right\rangle+\delta t\left\langle f^{k+1},U^{k+1}\right\rangle.\end{aligned}$$

Considering the Cauchy–Schwarz inequality, one obtains

$$\begin{aligned}&\|U^{k+1}\|^2+\mu_1\|\nabla U^{k+1}\|^2+\mu_2\|\nabla U^{k+1}\|^2\\&\leqslant\left\langle U^k,U^{k+1}\right\rangle+\mu_1\sum_{j=0}^{k-1}(\lambda_{j+1}-\lambda_j)\left[\|\nabla U^{k+1}\|^2+\|\nabla U^{k-j}\|^2\right]\\&\quad+\mu_2\sum_{j=0}^{k-1}(\omega_{j+1}-\omega_j)\left[\|\nabla U^{k+1}\|^2+\|\nabla U^{k-j}\|^2\right]+\delta t\|f^{k+1}\|\|U^{k+1}\|.\end{aligned}$$

or

$$\begin{aligned}&\|U^{k+1}\|^2+\mu_1\|\nabla U^{k+1}\|^2+\mu_2\|\nabla U^{k+1}\|^2\\&\leqslant\|\tfrac{1}{2}U^k\|^2+\tfrac{1}{2}U^{k+1}\|^2+\tfrac{1}{2}\mu_1\sum_{j=0}^{k-1}(\lambda_j-\lambda_{j+1})\left[\|\nabla U^{k-j}\|^2+\|\nabla U^{k+1}\|^2\right]\\&\quad+\tfrac{1}{2}\mu_2\sum_{j=0}^{k-1}(\omega_j-\omega_{j+1})\left[\|\nabla U^{k-j}\|^2+\|\nabla U^{k+1}\|^2\right]+\delta t\|f^{k+1}\|\|U^{k+1}\|\\&\quad+\tfrac{\mu_1}{2}(1-\lambda_k)\|\nabla U^{k+1}\|^2+\tfrac{\mu_2}{2}(1-\omega_k)\|\nabla U^{k+1}\|^2.\end{aligned}$$

Regarding Lemma 2, we can write

$$\mu_1\lambda_k-\eta_{k+1}\geqslant 0,\qquad \mu_2\omega_k-\xi_{k+1}\geqslant 0.$$

Also, in view of Cauchy–Schwarz inequality, we obtain

$$\begin{aligned}&\|U^{k+1}\|^2+\mu_1\|\nabla U^{k+1}\|^2+\mu_2\|\nabla U^{k+1}\|^2\\&\leqslant\|\tfrac{1}{2}U^k\|^2+\tfrac{1}{2}\|U^{k+1}\|^2+\tfrac{1}{2}\mu_1\sum_{j=0}^{k-1}\lambda_j\|\nabla U^{k-j}\|^2\\&-\tfrac{1}{2}\mu_1\sum_{j=1}^{k}\lambda_j\|\nabla U^{k+1-j}\|^2+\tfrac{\mu_1}{2}(1-\lambda_k)\|\nabla U^{k+1}\|^2+\tfrac{1}{2}\mu_2\sum_{j=0}^{k-1}\omega_j\|\nabla U^{k-j}\|^2\\&-\tfrac{1}{2}\mu_2\sum_{j=1}^{k}\omega_j\|\nabla U^{k+1-j}\|^2+\tfrac{\mu_2}{2}(1-\omega_k)\|\nabla U^{k+1}\|^2+\delta t\|f^{k+1}\|\|U^{k+1}\|\\&+\tfrac{\mu_1\lambda_k-\eta_{k+1}}{2}\|\nabla U^0\|^2+\tfrac{\mu_1\lambda_k-\eta_{k+1}}{2}\|\nabla U^{k+1}\|^2\\&+\tfrac{\mu_2\omega_k-\xi_{k+1}}{2}\|\nabla U^0\|^2+\tfrac{\mu_2\omega_k-\xi_{k+1}}{2}\|\nabla U^{k+1}\|^2.\end{aligned}$$

According to the Poincaré and Young's inequalities, we get

$$\|U^{k+1}\|\leqslant C\|\nabla U^{k+1}\|,$$

$$\forall\theta\neq 0\longrightarrow|ab|\leqslant\frac{1}{2\theta^2}a^2+\frac{\theta^2}{2}b^2,$$

respectively, and we obtain

$$\begin{aligned}&\|U^{k+1}\|^2+\mu_1\|\nabla U^{k+1}\|^2+\mu_2\|\nabla U^{k+1}\|^2\\&\leqslant\|\tfrac{1}{2}U^k\|^2+\tfrac{1}{2}\|U^{k+1}\|^2+\tfrac{1}{2}\mu_1\sum_{j=0}^{k}\lambda_j\|\nabla U^{k-j}\|_1^2\\&+\tfrac{1}{2}\mu_2\sum_{j=0}^{k}\omega_j\|\nabla U^{k-j}\|^2-\tfrac{1}{2}\mu_1\sum_{j=0}^{k+1}\lambda_j\|\nabla U^{k+1-j}\|^2-\tfrac{1}{2}\mu_2\sum_{j=0}^{k+1}\omega_j\|\nabla U^{k+1-j}\|^2\\&+(\tfrac{\mu_1}{2}+\tfrac{\mu_2}{2})\|\nabla U^{k+1}\|^2+(\tfrac{\mu_1}{2}+\tfrac{\mu_2}{2})\|\nabla U^{k+1}\|^2+\tfrac{1}{2}\tfrac{C^2\delta t^2}{\xi_{k+1}+\eta_{k+1}}\|f^{k+1}\|^2.\end{aligned}$$

After simplification, we arrive at

$$\begin{aligned}&\tfrac{1}{2}\|U^{k+1}\|^2+\tfrac{\mu_1}{2}\sum_{j=0}^{k+1}\lambda_j\|\nabla U^{k+1-j}\|^2+\tfrac{\mu_2}{2}\sum_{j=0}^{k+1}\lambda_j\|\nabla U^{k+1-j}\|^2\\&\leqslant\tfrac{1}{2}\|U^k\|^2+\tfrac{\mu_1}{2}\sum_{j=0}^{k}\lambda_j\|\nabla U^{k-j}\|^2+\tfrac{\mu_2}{2}\sum_{j=0}^{k}\omega_j\|\nabla U^{k-j}\|^2\\&\quad+\tfrac{1}{2}\tfrac{C^2\delta t^2}{\xi_{k+1}+\eta_{k+1}}\|f^{k+1}\|^2.\end{aligned}$$

Therefore, we obtain

$$\begin{aligned}\zeta^{k+1} &\leqslant \zeta^{k} + \tfrac{C^2\delta t^2}{\xi_{k+1}+\eta_{k+1}}\|f^{k+1}\|^2 \\ &\leqslant \zeta^{0} + \sum_{j=0}^{k}\tfrac{C^2\delta t^2}{\xi_{j+1}+\eta_{j+1}}\|f^{j+1}\|^2 \\ &\leqslant \zeta^{0} + \tfrac{C^2\delta t T}{\xi_{k+1}+\eta_{k+1}}\max_{0\leqslant j\leqslant k}\|f^{j+1}\|^2,\end{aligned} \tag{8}$$

where

$$\zeta^{k} = \|U^{k}\|^2 + \mu_1\sum_{j=0}^{k}\lambda_j\|\nabla U^{k-j}\|^2 + \mu_2\sum_{j=0}^{k}\omega_j\|\nabla U^{k-j}\|^2.$$

If we consider

$$\zeta^{0} = \|U^{0}\|^2 + \mu_1\|\nabla U^{0}\|^2 + \mu_2\|\nabla U^{0}\| = \|U^{0}\|^2_{H^1(\Omega)},$$

then expression (8) can be rewritten as

$$\|U^{k+1}\|_{H^1(\Omega)} \leqslant \|U^{0}\|_{H^1(\Omega)} + \left(\frac{C^2\delta t T}{\xi_{k+1}+\eta_{k+1}}\right)^{\frac{1}{2}}\max_{0\leqslant j\leqslant k}\|f^{j+1}\|^2, \quad k\geqslant 0. \tag{9}$$

From [53], for $k \geqslant 0$, it holds that

$$\begin{aligned}\tfrac{T\delta t}{\xi_{k+1}+\eta_{k+1}} &= \tfrac{T\delta t\Gamma(\alpha+1)(k+1)^{1-\alpha}}{\delta t^{\alpha}} \leqslant T^{2-\alpha}\Gamma(\alpha),\\ \tfrac{T\delta t}{\xi_{k+1}+\eta_{k+1}} &= \tfrac{T\delta t\Gamma(\beta+1)(k+1)^{1-\beta}}{\delta t^{\beta}} \leqslant T^{2-\beta}\Gamma(\beta).\end{aligned}$$

In view of the aforesaid inequalities and the relation (9), we get

$$\|U^{k+1}\|_{H^1(\Omega)} \leqslant \|U^{0}\|_{H^1(\Omega)} + \widetilde{C}\,T^{1-\frac{\min\{\alpha,\beta\}}{2}}\max_{0\leqslant j\leqslant k}\|f^{j+1}\|^2,$$

and the proof is concluded. □

Theorem 2. Let $u^{k+1} = u(\mathbf{x}, t_{k+1}) \in H^1(\Omega)$ represent the exact solution of Eqs. (1)–(3) and U^{k+1} be the approximate solution obtained by (6). Then, the semi-implicit difference algorithm (6) has convergence rate $\mathcal{O}\left(\delta t^{1+\min\{\alpha,\beta\}}\right)$.

Proof. We define $\rho^{k+1} = u^{k+1} - U^{k+1}$ at $t = t_{k+1},\ k = 0, 1, \ldots, M$. By subtracting Eq. (5) from Eq. (6), we obtain

$$\begin{aligned}\rho^{k+1} - (\mu_1+\mu_2)\Delta\rho^{k+1} = \rho^{k} &+ \mu_1\sum_{j=0}^{k-1}(\lambda_{j+1}-\lambda_j)\Delta\rho^{k-j} \\ &+ \mu_2\sum_{j=0}^{k-1}(\omega_{j+1}-\omega_j)\Delta\rho^{k-j} + \delta t R^{k+1},\end{aligned} \tag{10}$$

where $|R^{k+1}| \leqslant \delta t^{1+\min\{\alpha,\beta\}})$ and $\rho^0 = 0$. Regarding Theorem 1 and Eq. (10), the following inequality is obtained:

$$\|\rho^{k+1}\|_{H^1(\Omega)} \leqslant \widetilde{C}\,T^{1-\frac{\delta t^{\min\{\alpha,\beta\}}}{2}}\delta t^{1+\min\{\alpha,\beta\}},$$

which finishes the proof of Theorem 2. □

Local hybridization of the Gaussian and cubic kernels

The RBF is a value dependent function on the distance from the center point. The RBF can be easily implemented by using the distance functions to solve multi-dimensional PDE. In the RBF method, the approximation of the function $u(\mathbf{x})$ to the data values $u_j = u(\mathbf{x}_j), j = 1, \ldots, N$, at the centers $X_C = \{\mathbf{x}_1, \ldots, \mathbf{x}_N\} \subseteq \mathbb{R}^d$, is represented as

$$u(\mathbf{x}) \simeq S(\mathbf{x}) = \sum_{j=1}^{N}\beta_j\phi_j(\mathbf{x}, \varepsilon), \tag{11}$$

where β_j are unknown coefficients, $\phi_j(\mathbf{x}, \varepsilon) = \phi(\|\mathbf{x} - \mathbf{x}_j\|_2, \varepsilon), j = 1, \ldots, N$, are RBF, $r = \|\mathbf{x} - \mathbf{x}_j\|$ is the Euclidean norm between $\mathbf{x}$ and $\mathbf{x}_j$, and ε denotes shape parameter. The unknown expansion coefficients, $\{\beta_j\}_{j=1}^{N}$, are determined by imposing the interpolation condition $S(\mathbf{x}_i^c) = u_i^c, \quad i = 1, \ldots, N$ [54,55].

Mishra et al. [56] first introduced the hybrid Gaussian-cubic RBF as a stable method for interpolation problems involving scattered data. Later, Mishra et al. [57,58] developed a stabilized RBF-FD approach with a hybrid kernel, generated through the cubic and Gaussian RBF hybridization based on FD. It was shown that this hybrid kernel was able to calculate stable interpolants for scattered nodes when there were a large number of degrees of freedom. In addition, the ill-conditioning in the numerical solution of PDEs was reduced. The hybrid Gaussian-cubic kernel is expressed by the relationship:

$$\phi(r, \varepsilon) = c_1\exp(-\varepsilon^2 r^2) + c_2 r^3, \tag{12}$$

with c_1 and c_2 representing the weights that control the Gaussian and cubic kernels, respectively, and ε standing for the shape parameter of the Gaussian kernel

$$\phi(r, \varepsilon) = \exp(-\varepsilon^2 r^2) + \vartheta r^3, \tag{13}$$

where the parameters ε and $\vartheta = c_2/c_1$ play a significant role in the stability and accuracy of the proposed technique. The parameters that control the cubic and Gaussian kernels in the hybrid RBF are chosen via global particle swarm optimization. The proposed strategy was observed to considerably decrease the ill-conditioning in the global RBF (GRBF) collocation technique. Moreover, it maintains the accuracy and stability for considerably small shape parameters. The term "stabilized" can be interpreted in two ways here [57,58]. On one hand, it can refer to the significant reduction in the interpolation matrix condition number. On the other hand, it can also point to the stabilization of the eigenvalue spectra of the system matrix belonging to the linear system irrespective of the stencil size or any stencil irregularity. This hybrid RBF overcomes the ill-conditioning issue in RBF-FD and results in a stabilized evaluation for a low computational cost, equivalent to the evaluation obtained from the GRBF. The proposed strategy decreases considerably the ill-conditioning in the GRBF. Moreover, it maintains the accuracy and stability for considerably small shape parameters [57,58]. Oruç [59] applied the local hybrid kernel meshless method to approximate the fractional cable equation.

Kansa [60,61] adopted a linear differential operator $\mathscr{L}$ for interpolating (11) in order approximate $\mathscr{L}u$ at the N scatter nodes,

$$\mathscr{L}u(\mathbf{x}_i) \simeq \sum_{j=1}^{N}\beta_j\mathscr{L}\phi_j(\mathbf{x}_i, \varepsilon). \tag{14}$$

Eq. (14) represents a GRBF approximation since one needs all points in the domain to approximate $\mathscr{L}$ at one of the points. That is to say, in order to determine the interpolation coefficient, one needs to consider all the spatial domain points. However, a large and ill-conditioned linear system is generated in the GRBF, which may leads to uncertain results. On the other hand, one can use the local RBF method only for the local support domain (restricted nodes) on each center rather than for the whole set of points. The local RBF results in a sparse and better-conditioned linear system and, at the same time, is reliable for ill-conditioned problems.

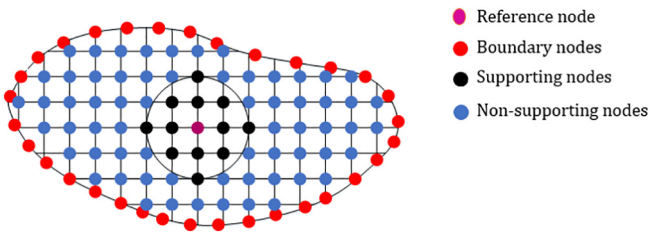

Fig. 1. The adopted stencil in the two-dimensional case based on the center point and its support.

Suppose that $\Xi = \{\mathbf{x}_1, \ldots, \mathbf{x}_N\} \subseteq \mathbb{R}^d$ is a set of N distinct points computational region Ω that splits into two sets I and B, which are the indices of the internal and boundary nodes, respectively, and that N denotes the total number of nodes so that $N = N_I + N_B$. Moreover, consider the subset $\Xi^i = \left\{\mathbf{x}_1^{(i)}, \ldots, \mathbf{x}_{N_s}^{(i)}\right\} \subseteq \Xi$ that is a vector with center $\mathbf{x}_i$ that including the center number and the indices of the $N_s - 1$ nearest neighboring centers. Each center and its $N_s - 1$ neighbors are named a stencil. Fig. 1 represents a typical stencil. Our target of this part is to approximate the Laplacian operator $\Delta u(\mathbf{x}) = \frac{\partial^2 u}{\partial x^2} + \frac{\partial^2 u}{\partial y^2}$ through the proposed method, where $\mathbf{x} = (x, y)^T$. The linear differential operator Δ at a reference node $\mathbf{x}_i$ can be approximated using the weighted linear sum of function values at all nodes in its support domain as:

$$\Delta u(\mathbf{x}_i) \simeq \sum_{j=1}^{N_s} w_j^{(i)} u\left(\mathbf{x}_j^{(i)}\right). \tag{15}$$

The LRBF-FD stencil weights, $\left\{w_j^{(i)}\right\}_{j=1}^{N_s}$, will be computed by enforcing the linear constraint (15) and the RBF $\{\phi_j(\mathbf{x}, \varepsilon)\}_{j=1}^{N_s}$, centered at the stencil point locations [42,62,63], that can be formulated as

$$\Delta\phi_k(\mathbf{x}_i, \varepsilon) = \sum_{j=1}^{N_s} w_j^{(i)} \phi_j(\mathbf{x}_k, \varepsilon), \quad k = 1, \ldots, N_s. \tag{16}$$

Therefore, we have a system of equations with size $N_s \times N_s$ at each stencil as follows

$$\Phi \mathbf{w}^{(i)} = \Psi^{(i)}, \tag{17}$$

where $\phi_{kj} = \phi_j(\mathbf{x}_k, \varepsilon), \quad k, j = 1, \ldots, N_s$, are the elements of the coefficient matrix Φ , $\mathbf{w}_{N_s \times 1}^{(i)} = \left\{w_j^{(i)}\right\}_{j=1}^{N_s}$, is differentiation weights for the point $\mathbf{x_i}$, and $\Psi_{N_s \times 1}^{(i)}$ has the elements $\Delta\phi_k(\mathbf{x}_i, \varepsilon), \quad k = 1, \ldots, N_s$. The weight coefficients $\mathbf{w}^{(i)}$ on the corresponding local domain can be calculated as

$$\mathbf{w}^{(i)} = \Phi^{-1}\Psi^{(i)}. \tag{18}$$

Solving Eq. (18) and substituting the obtained result into Eq. (15) gives the approximation solution of the linear differential operator, that is, gives Δ at node $\mathbf{x}_i$. The following system of equations can be integrated by substituting (15) into Eq. (6) at an internal point $\mathbf{x}_i = (x_i, y_i)$ and Eq. (3) at all Dirichlet boundary points as

$$\begin{aligned}\mathbf{A}\mathbf{U}^{n+1} = \mathbf{B}\mathbf{U}^n &+ \mu_1 \sum_{k=0}^{n-1} (\lambda_{k+1} - \lambda_k)\mathbf{C}\mathbf{U}^{n-k} \\ &+ \mu_2 \sum_{k=0}^{n-1} (\omega_{k+1} - \omega_k)\mathbf{D}\mathbf{U}^{n-k} + \mathbf{b},\end{aligned} \tag{19}$$

where the elements of the matrices $\mathbf{A}, \mathbf{B}, \mathbf{C}, \mathbf{D}$ and $\mathbf{b}$ can be written as follows:

$$\mathbf{A}_{ij} = \begin{cases} \delta_{ij} - \mu w_j^{(i)}, & i = 1, \ldots, N_I, j = 1, \ldots, N, \\ \delta_{ij}, & i = N_I + 1, \ldots, N, j = 1, \ldots, N, \end{cases}$$

$$\mathbf{B}_{ij} = \begin{cases} \delta_{ij}, & i = 1, \ldots, N_I, j = 1, \ldots, N, \\ 0, & i = N_I + 1, \ldots, N, j = 1, \ldots, N, \end{cases}$$

$$\mathbf{C}_{ij} = \begin{cases} w_j^{(i)}, & i = 1, \ldots, N_I, j = 1, \ldots, N, \\ 0, & i = N_I + 1, \ldots, N, j = 1, \ldots, N, \end{cases}$$

$$\mathbf{D}_{ij} = \begin{cases} w_j^{(i)}, & i = 1, \ldots, N_I, j = 1, \ldots, N, \\ 0, & i = N_I + 1, \ldots, N, j = 1, \ldots, N, \end{cases}$$

$$\mathbf{b} = \begin{cases} \tau f_i^{n+1}, & i = 1, \ldots, N_I, \\ g^{n+1}(\mathbf{x}_i), & i = N_I + 1, \ldots, N, \end{cases}$$

$$\mathbf{U}^n = (U^n(\mathbf{x}_1), U^n(\mathbf{x}_2), \ldots, U^n(\mathbf{x}_N))^T.$$

Moreover, we have $\mu = \mu_1 + \mu_2$ and δ_{ij} for the Kronecker delta function. The implementation of the proposed method, underlying computational aspects, can be summarized as follows:

Step 1 `Generate nodes distributions`
The uniform or Halton node distributions are generated in the solution domain as the set of evaluation points. The uniformly random Halton nodes are generated by using the MATLAB program *haltonseq.m* [64]. The set $\Omega = \{\mathbf{x}_1, \ldots, \mathbf{x}_N\}$ of collocation nodes and is splited into two sets I and B, which are the indices of the internal and boundary nodes, respectively, and where N denotes the total number of nodes so that $N = N_I + N_B$.

Step 2 `Construction of the support domain`
For each $\mathbf{x}_i$, we first create a local support domain $\Xi^i = \left\{\mathbf{x}_1^{(i)}, \ldots, \mathbf{x}_{N_s}^{(i)}\right\}$ that includes the nearest $N_s - 1$ evaluation points to $\mathbf{x}_i$. In this approach, each local support domain includes only evaluation nodes. The neighboring points can be selected via several methods. One of these methods consists of defining a finite radius around a node and assuming that the points within that radius are the corresponding neighboring points. One can achieve the `kd-tree` with the help of the `knnsearch` function available in MATLAB [65,64].

Step 2 `Determination of the differentiation weights for the point` $\mathbf{x}_i$
The weight coefficients $\mathbf{w}^{(i)}$ are obtained to approximate the Laplacian operator Δ on the corresponding local domain in the center $\mathbf{x}_i$ by using the relation (18).

Step 3 `Create the coefficient matrix`
We create the matrices $\mathbf{A}, \mathbf{B}, \mathbf{C}$ and $\mathbf{D}$ by using **Step** 2.

Step 4 `Calculate the approximate solution in the main time stepping loop`
We set Eq. (19) in a loop for the number of time steps, $n = 1, \ldots, M$, and we calculate the approximate solution U^n at each time step.

Numerical examples

This section includes three problems and four domains for illustrating the effectiveness and accuracy of the proposed method. In order to assess the performance, we calculate the time convergence order by means of the formula:

$$C_{\delta t} = \log_2\left(\frac{\|L_\infty(2\delta t, h)\|}{\|L_\infty(\delta t, h)\|}\right),$$

where $L_\infty = \max_{1\leqslant j\leqslant N-1} |U(x_j,T) - u(x_j,T)|$ denotes the absolute error. The condition number (C-N) of the coefficient matrix is evaluated by means of the Matlab command `condest`. All computations are obtained in MATLAB R2016a on a Pentium IV, 2800 MHz CPU with 8 Gbyte memory. Fig. 2 considers four distinct types of computational regions $(\Omega_i, i = 1,2,3,4)$. The domain $\Omega_1 = [0,1]^2$ is discretized including the uniform points. The contour of Ω_2 is determined by the polar form $r(\theta) = \frac{1}{9}(17 - 8\cos(3\theta))$, $0 \leqslant \theta \leqslant 2\pi$. The domains Ω_3 and Ω_4 exhibit irregular geometries given by $r(\theta) = \sqrt{\sin^2(5\theta) + \sin^2(2\theta) + \cos^2(\theta)}$ and $r(\theta) = \sqrt[3]{\cos(3\theta) + \sqrt{2 - \sin^2(3\theta)}}, 0 \leqslant \theta \leqslant 2\pi$, respectively, discretized with irregular distribution of nodes.

Example 1. Consider the following MTFDE:

$$\begin{aligned}\tfrac{\partial u(x,y,t)}{\partial t} \quad & -\mathrm{D}_t^{1-\alpha}\Delta u(x,y,t) - \mathrm{D}_t^{1-\beta}\Delta u(x,y,t)\\ & = \exp(x+y)\Big[(1+\alpha+\beta)t^{\alpha+\beta} - 2\tfrac{\Gamma(2+\alpha+\beta)}{\Gamma(1+2\alpha+\beta)}t^{2\alpha+\beta}\\ & -2\tfrac{\Gamma(2+\alpha+\beta)}{\Gamma(1+\alpha+2\beta)}t^{\alpha+2\beta}\Big], \qquad (x,y)\in\Omega, \qquad 0 < t \leqslant T.\end{aligned}$$

The boundary and initial conditions are obtained from the analytic solution $u(x,y,t) = \exp(x+y)t^{1+\alpha+\beta}$.

The new method is employed for determining the solution with different values of ε, ϑ, $\delta t, \alpha, \beta$ and N on the four domains. The numerical results are summarised in Tables 1–4 and Figs. 3–6. Tables 1 and 2 list the rates of convergence in the temporal direction at $T = 1$ on the domains $\{\Omega_1, \Omega_2, \Omega_3, \Omega_4\}$ with

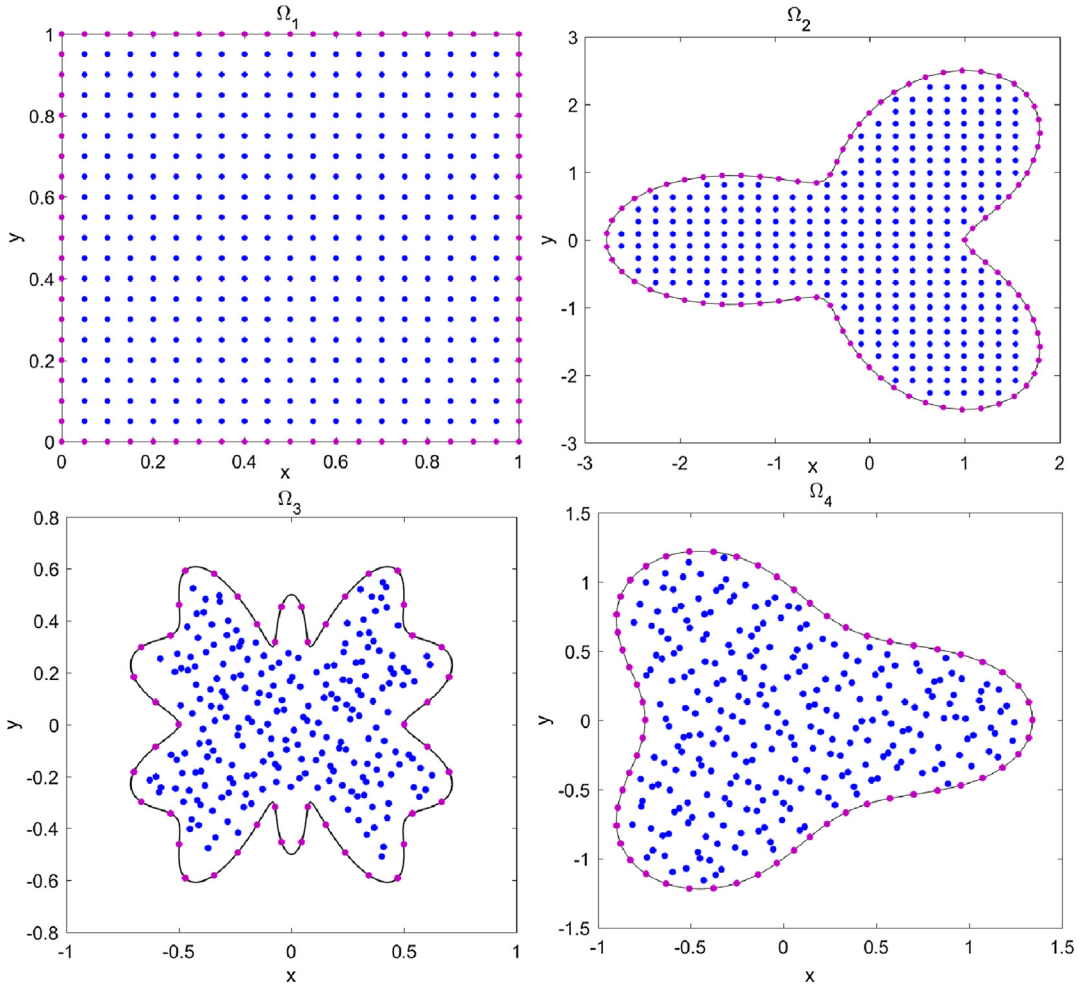

Fig. 2. The computational regions $\{\Omega_1, \Omega_2, \Omega_3, \Omega_4\}$ for the test problems.

Table 1
Numerical orders of convergence in the time variable with $\{\alpha, \beta\} = \{0.6, 0.9\}$ on domains Ω_1 and Ω_2.

δt	Ω_1		Ω_2	
	L_∞	$C_{\delta t}$	L_∞	$C_{\delta t}$
1/10	2.1945e − 03	–	6.3279e − 03	–
1/20	7.9646e − 04	1.4622	2.3805e − 03	1.4105
1/40	2.8314e − 04	1.4921	8.0166e − 03	1.4829
1/80	9.5490e − 05	1.5681	2.7344e − 03	1.5518
1/160	3.2082e − 05	1.5736	8.9587e − 04	1.6099
1/320	1.0377e − 05	1.6284	2.9213e − 04	1.6167
1/640	3.3887e − 06	1.6146	9.1815e − 05	1.6698
1/1280	1.1043e − 06	1.6176	2.9825e − 05	1.6222

Table 2
Numerical orders of convergence in the time variable with $\{\alpha,\beta\}=\{0.6,0.9\}$ on domains Ω_3 and Ω_4 of Example 1.

δt	Ω_3		Ω_4	
	L_∞	$C_{\delta t}$	L_∞	$C_{\delta t}$
1/10	$3.6339e-03$	–	$4.1765e-03$	–
1/20	$1.2596e-03$	1.5286	$1.5332e-03$	1.4457
1/40	$4.2525e-04$	1.5666	$5.2825e-04$	1.5373
1/80	$1.4188e-04$	1.5836	$1.7552e-04$	1.5896
1/160	$4.6799e-05$	1.6001	$5.7206e-05$	1.6174
1/320	$1.4833e-05$	1.6577	$1.8761e-05$	1.6084
1/640	$4.8304e-06$	1.6186	$6.0341e-06$	1.6365
1/1280	$3.3887e-06$	1.6146	$9.1815e-05$	1.6698

Table 3
The L_∞ error for the schemes described in [31,34] and the proposed method at $T=1$ on Ω_1 of Example 1.

δt	Ref. [31]		Ref. [34]		Proposed method	
	L_∞	$C_{\delta t}$	L_∞	$C_{\delta t}$	L_∞	$C_{\delta t}$
1/4	$1.1481e-002$	–	$1.1093e-002$	–	$1.0635e-02$	–
1/8	$3.2554e-003$	1.8183	$2.9286e-003$	1.9214	$2.9948e-03$	1.8283
1/16	$5.0574e-004$	2.6864	$4.2727e-004$	2.7769	$3.8861e-04$	2.9461
1/32	$2.3165e-004$	1.1264	$1.6510e-004$	1.3718	$1.5721e-04$	1.3056
1/64	–	–	–	–	$6.5273e-05$	1.2681
1/128	–	–	–	–	$2.7591e-05$	1.2423
1/256	–	–	–	–	$1.1874e-05$	1.2164

Table 4
The L_∞ error, C-N and CPU time (in seconds) of Example 1.

N_s	Ω_3			Ω_4		
	L_∞	C-N	CPU	L_∞	C-N	CPU(s)
43	$7.1436e-03$	$3.4725e+04$	6.451	$2.4877e-04$	$5.1020e+05$	6.616
63	$3.6694e-03$	$3.7118e+04$	11.172	$1.0377e-04$	$5.0928e+05$	11.983
83	$9.0852e-04$	$3.8164e+04$	15.302	$9.2497e-05$	$5.2278e+05$	15.443
103	$4.0743e-04$	$3.9388e+04$	22.081	$4.6659e-05$	$5.2502e+05$	22.465

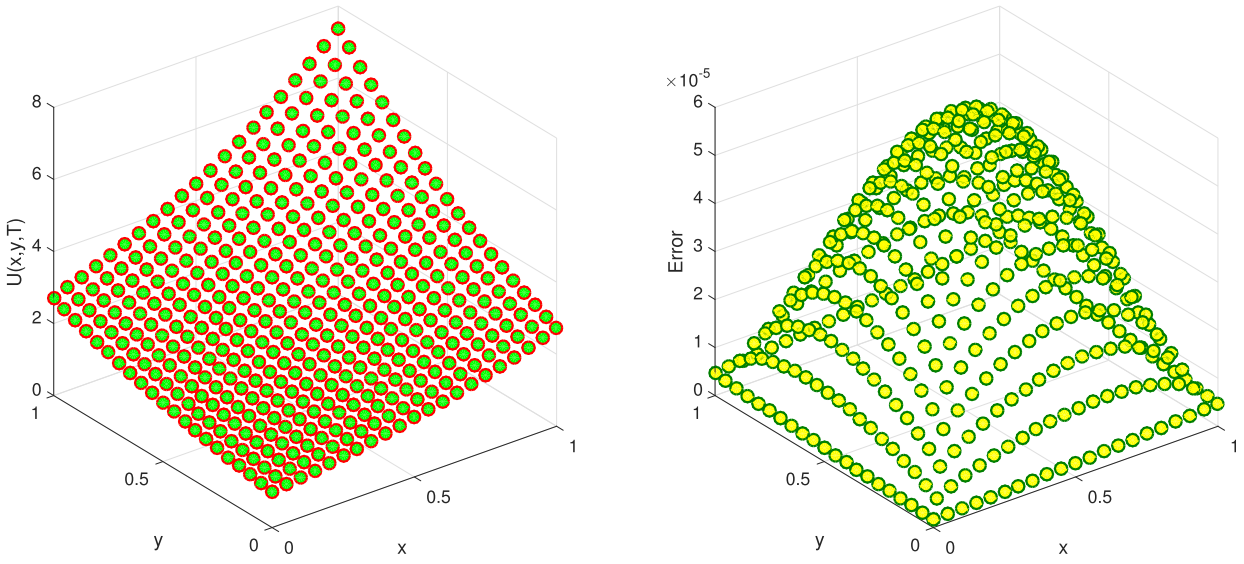

Fig. 3. The numerical solutions and the resulting errors at final time $T=1$ on region Ω_1 of Example 1.

$\varepsilon=2.1,\vartheta=0.00001,N_s=75$, and $N=325$. From these tables, it can be observed that the rate of convergence in the temporal variable is $\mathcal{O}\left(\delta t^{1+\min\{\alpha,\beta\}}\right)$, which is compatible with the theoretical formulation. Table 3 compares the computational errors of the proposed technique with those obtained by other methods [31,34] for $\{\alpha,\beta\}=\{0.5,0.2\}$. These results are in agreement with those reported in [31,34]. Table 4 lists the computational errors, the condition number and computational time (in seconds) for different stencil sizes N_l with $\varepsilon=2.1,\vartheta=0.00055,\{\alpha,\beta\}=\{0.7,0.4\},\delta t=1/500$. It can be concluded that the L_∞ error dimin-

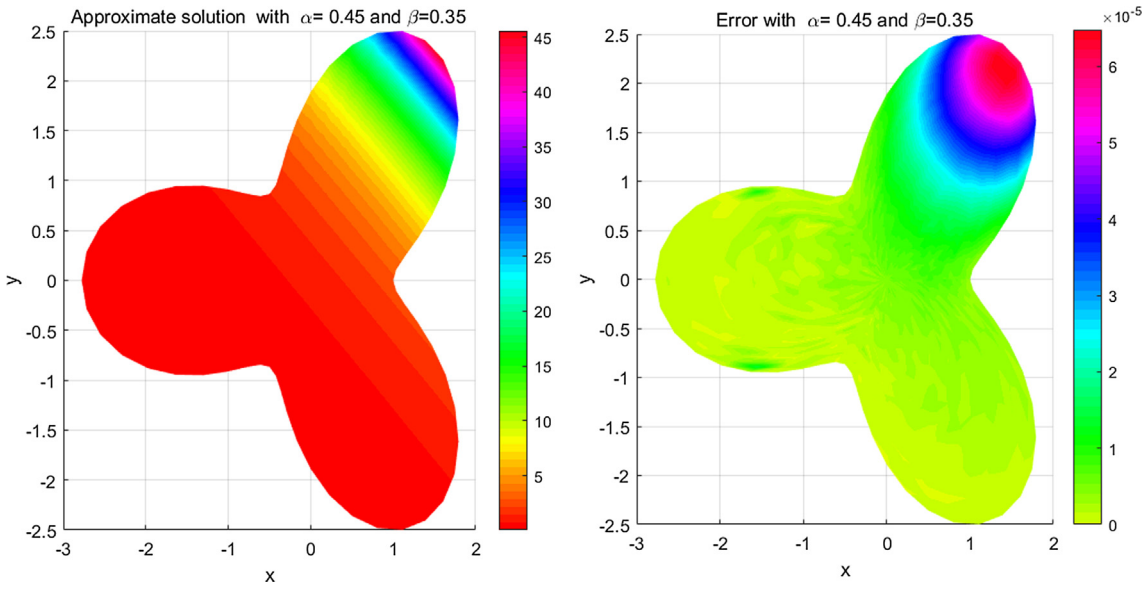

Fig. 4. The numerical solutions and the resulting errors at final time $T = 1$ on region Ω_2 of Example 1.

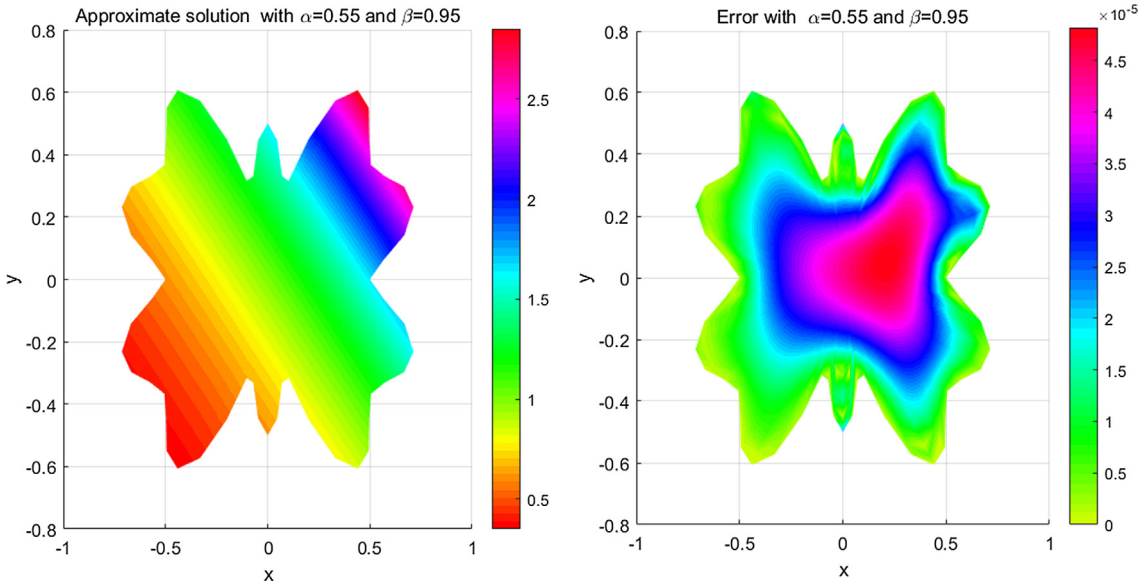

Fig. 5. The numerical solutions and the resulting errors at final time $T = 1$ on region Ω_3 of Example 1.

ishes by increasing the stencil sizes N_l. Furthermore, the condition numbers are quite acceptable. Table 5 compares the L_∞ error for the schemes described in [30] with those obtained by the proposed technique when $T = 1$ on Ω_1. Table 6 demonstrates the L_∞ error for the proposed technique at different final time T on Ω_1. From this table, it can be seen that the numerical results are acceptable in larger T. Fig. 3 represents the numerical solutions and the computational errors by letting $\varepsilon = 2.4, \vartheta = 0.0001, \{\alpha, \beta\} = \{0.5, 0.5\}$, $\delta t = 1/100, N_s = 33$ and $N = 289$, when $T = 1$ on Ω_1. Fig. 4 depicts the numerical solutions and the computational errors by taking $\varepsilon = 2.1, \vartheta = 0.00015, \{\alpha, \beta\} = \{0.45, 0.35\}, \delta t = 1/150, N_s = 73$ and $N = 401$, when $T = 1$ on Ω_2. Fig. 5 portrays the numerical solutions and the computational errors by letting $\varepsilon = 2.2, \vartheta = 0.000151$, $\{\alpha, \beta\} = \{0.55, 0.95\}, \delta t = 1/150, N_s = 67$ and $N = 521$, when $T = 1$ on Ω_3. Finally, Fig. 6 represents the numerical solutions and the computational errors by taking $\varepsilon = 2.5, \vartheta = 0.000055$, $\{\alpha, \beta\} = \{0.15, 0.75\}, \delta t = 1/150, N_s = 83$ and $N = 625$, when $T = 1$ on Ω_4. From Figs. 4–6, it can be seen that the proposed method performs well when solving problems involving complicated and irregular domains.

Example 2. Consider the following two-dimensional MTFDE:

$$\begin{aligned}\tfrac{\partial u(x,y,t)}{\partial t} \quad & -\mathrm{D}_t^{1-\alpha}\Delta u(x,y,t) - \mathrm{D}_t^{1-\beta}\Delta u(x,y,t) \\ & = \sin(x+y)\Big[(1+\alpha+\beta)t^{\alpha+\beta} + 2\tfrac{\Gamma(2+\alpha+\beta)}{\Gamma(1+2\alpha+\beta)}t^{2\alpha+\beta} \\ & +2\tfrac{\Gamma(2+\alpha+\beta)}{\Gamma(1+\alpha+2\beta)}t^{\alpha+2\beta}\Big], \qquad (x,y)\in\Omega, \qquad 0 < t \leqslant T.\end{aligned}$$

The boundary and initial conditions are calculated using the analytic solution $u(x,y,t) = \sin(x+y)t^{1+\alpha+\beta}$.

The proposed technique is adopted for computing the solution with various values of ε, ϑ, $\delta t, \alpha, \beta$ and N on $\Omega_i, i = 1, 2, 3, 4$. The

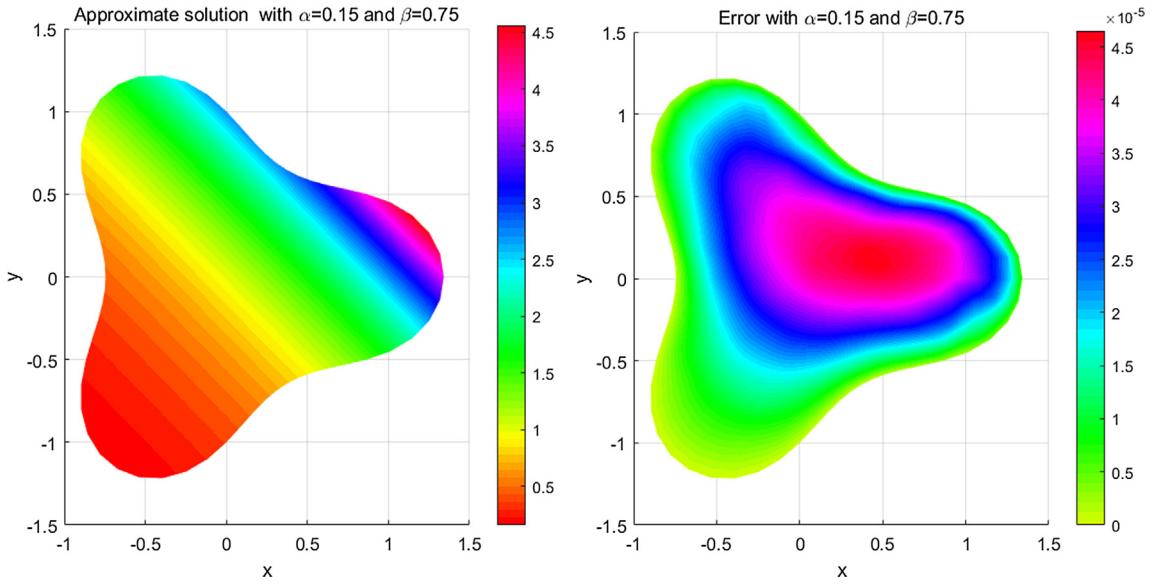

Fig. 6. The numerical solutions and the resulting errors at final time $T = 1$ on region Ω_4 of Example 1.

Table 5
The L_∞ error for the schemes described in [30] and the proposed method at $T = 1$ on Ω_1 of Example 1.

(α, β)	N	δt	Ref. [30]	Proposed method
$(0.1, 0.2)$	81	$1/64$	$8.1150e-03$	$1.0893e-03$
	289	$1/1024$	$2.9754e-04$	$7.0079e-05$
$(0.5, 0.8)$	81	$1/64$	$1.2422e-03$	$1.5288e-03$
	289	$1/1024$	$1.1255e-03$	$8.8765e-05$

Table 6
The L_∞ error at the various final times on Ω_1 with $N = 441$ and $\delta t = 1/80$ of Example 1.

T	L_∞	C-N	CPU(s)
0.25	$8.3437e-05$	$9.2621e+04$	0.751
0.50	$1.0555e-04$	$9.2621e+04$	0.979
0.75	$2.7365e-04$	$9.2621e+04$	1.299
1.00	$3.4154e-04$	$9.2621e+04$	1.668
1.25	$4.7164e-04$	$9.2621e+04$	2.087
1.50	$5.4350e-04$	$9.2621e+04$	2.611
1.75	$7.4821e-04$	$9.2621e+04$	3.131
2.00	$8.7651e-04$	$9.2621e+04$	3.763

Table 7
Numerical orders of convergence in the time variable with $\{\alpha, \beta\} = \{0.3, 0.8\}$ on domains Ω_1 and Ω_2 of Example 2.

δt	Ω_1		Ω_2	
	L_∞	$C_{\delta t}$	L_∞	$C_{\delta t}$
$1/10$	$3.6116e-03$	–	$5.5384e-03$	–
$1/20$	$1.5493e-03$	1.2210	$2.3126e-03$	1.2600
$1/40$	$6.5849e-04$	1.2344	$9.5471e-04$	1.2764
$1/80$	$2.7379e-04$	1.2661	$3.8803e-04$	1.2989
$1/160$	$1.1047e-04$	1.3094	$1.5645e-04$	1.3105
$1/320$	$4.4231e-05$	1.3166	$6.3182e-05$	1.3081
$1/640$	$1.7520e-05$	1.3361	$2.5233e-05$	1.3242
$1/1280$	$7.0384e-06$	1.3157	$1.0175e-05$	1.3103

Table 8
Numerical orders of convergence in the time variable with $\{\alpha, \beta\} = \{0.7, 0.5\}$ on domains Ω_3 and Ω_4 of Example 2.

δt	Ω_3			Ω_4		
	L_∞	$C_{\delta t}$	CPU (s)	L_∞	$C_{\delta t}$	CPU (s)
1/10	$3.5765e-03$	–	0.352	$4.3375e-03$	–	0.298
1/20	$1.3478e-03$	1.4079	0.401	$1.6282e-03$	1.4136	0.337
1/40	$5.0307e-04$	1.4218	0.546	$6.0520e-04$	1.4278	0.376
1/80	$1.8205e-04$	1.4664	0.602	$2.1945e-04$	1.4635	0.498
1/160	$6.5172e-05$	1.4820	1.930	$7.8313e-05$	1.4866	0.859
1/320	$2.2605e-05$	1.5276	2.176	$2.7658e-05$	1.5016	1.774
1/640	$7.7608e-06$	1.5424	3.341	$9.5447e-06$	1.5349	2.588

Table 9
The error L_∞, C-N and CPU time (in seconds) with $\delta t = 1/500$ and $N = 857$ of Example 2.

N_s	Ω_2			Ω_3		
	L_∞	C-N	CPU	L_∞	C-N	CPU(s)
37	$7.6294e-04$	$1.8611e+04$	6.352	$4.2745e-04$	$5.1576e+05$	5.422
57	$5.5539e-04$	$2.3097e+04$	12.820	$2.5233e-04$	$5.0639e+05$	11.219
77	$3.0384e-04$	$3.1927e+04$	17.452	$9.5042e-05$	$5.1611e+05$	16.015
97	$8.3628e-05$	$3.3489e+04$	26.523	$5.3608e-05$	$5.1793e+05$	24.836

Table 10
The L_∞ error at the various final times on Ω_1 with $N = 676$ and $\delta t = 1/80$ of Example 2.

T	L_∞	C-N	CPU(s)
0.25	$7.7525e-05$	$1.9095e+05$	1.435
0.50	$1.4909e-04$	$1.9095e+05$	1.835
0.75	$2.5460e-04$	$1.9095e+05$	2.263
1.00	$5.9131e-04$	$1.9095e+05$	2.920
1.25	$6.5221e-04$	$1.9095e+05$	3.630
1.50	$7.8056e-04$	$1.9095e+05$	4.449
1.75	$9.0255e-04$	$1.9095e+05$	5.337
2.00	$1.8387e-03$	$1.9095e+05$	6.270

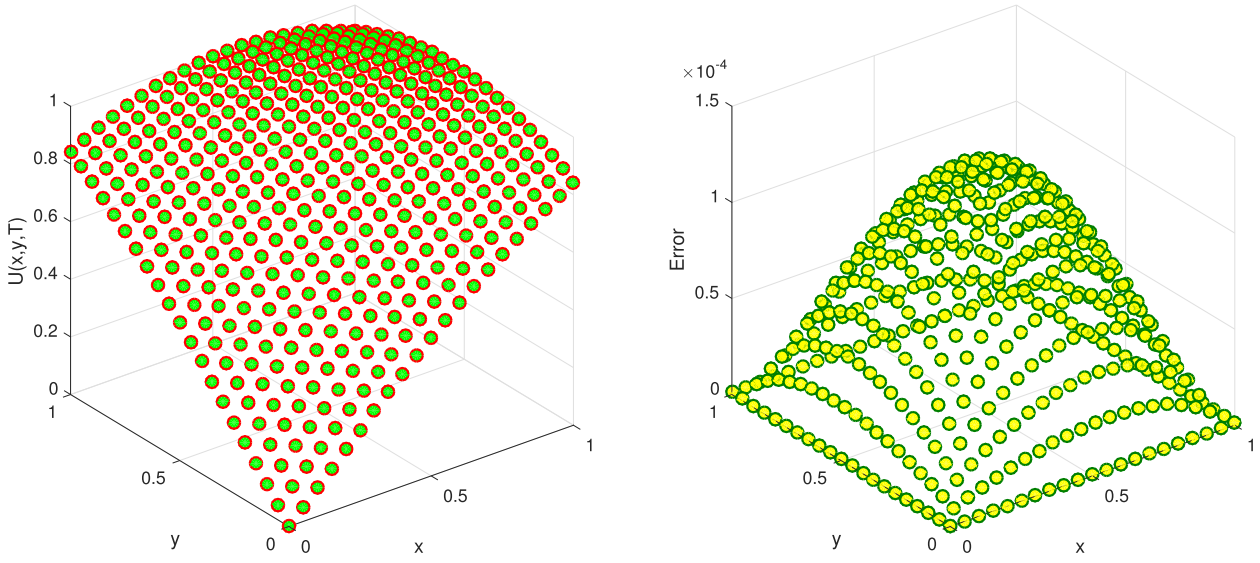

Fig. 7. The numerical solutions and the resulting errors for at final time $T = 1$ on region Ω_1 of Example 2.

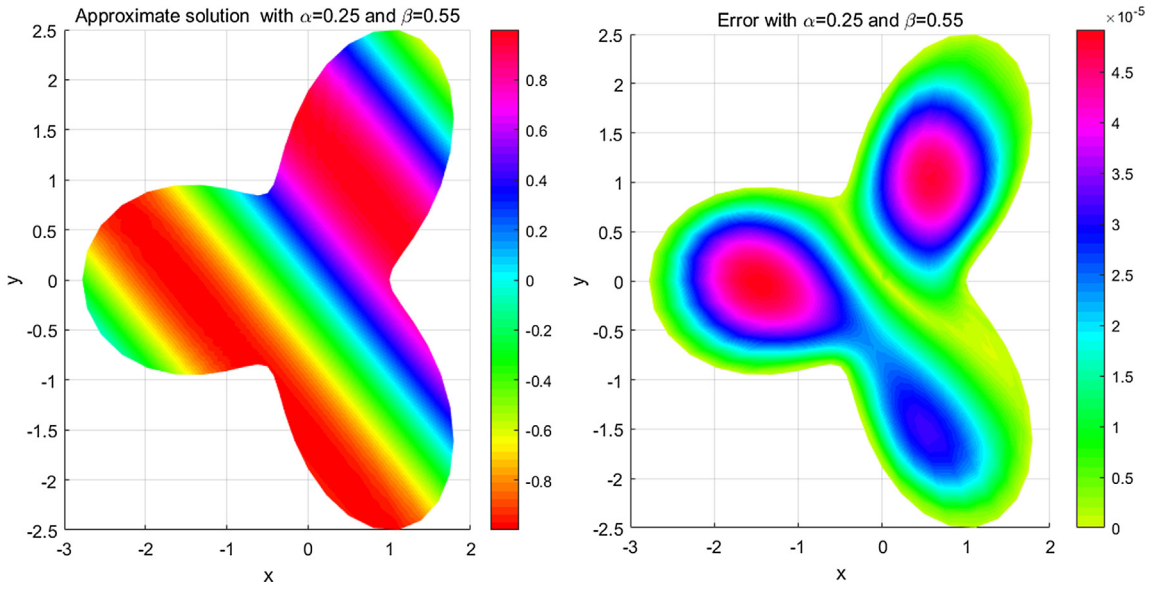

Fig. 8. The numerical solutions and the resulting errors at final time $T = 1$ on region Ω_2 of Example 2.

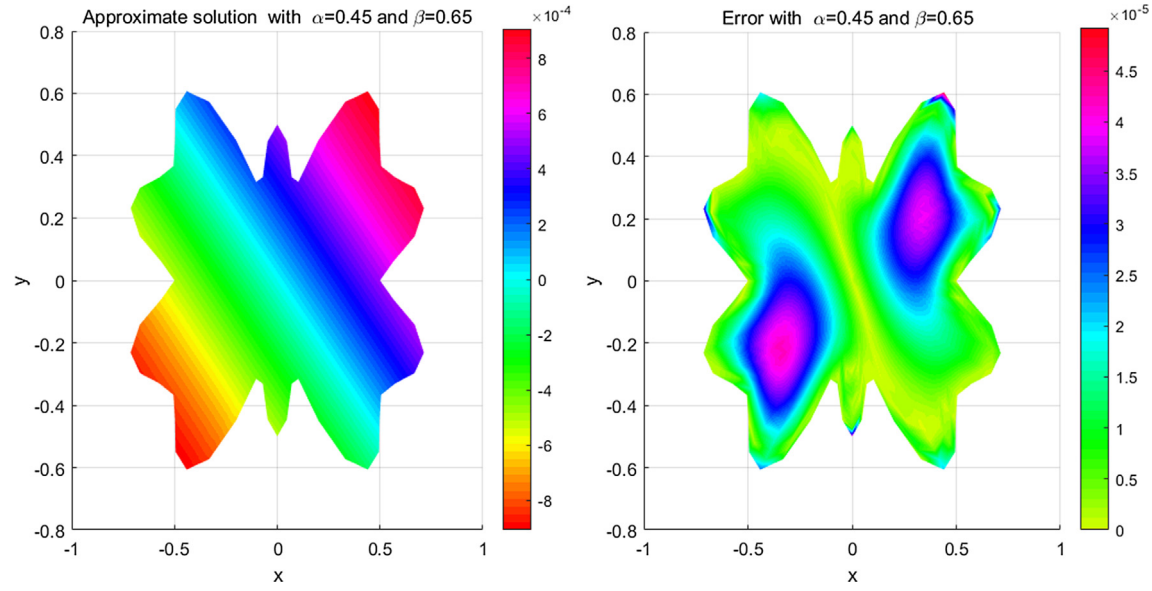

Fig. 9. The numerical solutions and the resulting errors at final time $T = 1$ on region Ω_3 of Example 2.

numerical results are given in Tables 7–10 and Figs. 7–10. Tables 7 and 8 illustrate the rate of convergence in the temporal direction at $T = 1$ on domains $\{\Omega_1, \Omega_2, \Omega_3, \Omega_4\}$ with $\varepsilon = 2.3, \vartheta = 0.00001$, $N_s = 43$ and $N = 275$. We can observe that the rate of convergence in temporal direction is $\mathcal{O}\left(\delta t^{1+\min\{\alpha,\beta\}}\right)$, which is compatible with the theoretical result. Table 9 reports the computational errors, the C-N and computational time (in seconds) for different stencil sizes N_l with $\varepsilon = 2.3, \vartheta = 0.00015, \{\alpha, \beta\} = \{0.3, 0.6\}$ and $\delta t = 1/500$. We observe that the L_∞ error diminishes by increasing the stencil sizes N_l, and that the condition numbers are quite acceptable. Table 10 lists the L_∞ error for the proposed technique at various final time T on Ω_1. It can be observed that the method yields accurate results in large T and exhibits adequate stability. Fig. 7 represents the numerical solutions and the computational errors by letting $\varepsilon = 2.0, \vartheta = 0.00005, \{\alpha, \beta\} = \{0.5, 0.5\}$, $\delta t = 1/100, N_s = 65$ and $N = 255$, when $T = 1$ on Ω_1. Fig. 8 portraits the numerical solutions and the computational errors by taking $\varepsilon = 2.1, \vartheta = 0.00055, \{\alpha, \beta\} = \{0.25, 0.55\}, \delta t = 1/150, N_s = 71$ and $N = 359$, when $T = 1$ on Ω_2. Fig. 9 plots the numerical solutions and the computational errors by letting $\varepsilon = 2.4, \vartheta = 0.000001$, $\{\alpha, \beta\} = \{0.45, 0.65\}, \delta t = 1/150, N_s = 59$ and $N = 431$, when $T = 1$ on Ω_3. Finally, Fig. 10 illustrates the numerical solutions and the computational errors by taking $\varepsilon = 2.5, \vartheta = 0.000055$, $\{\alpha, \beta\} = \{0.85, 0.35\}, \delta t = 1/150, N_s = 47$ and $N = 501$, when $T = 1$ on Ω_4. We verify that the accuracy of the proposed method is not affected by the complex shaped domains with the uniform and Halton nodes.

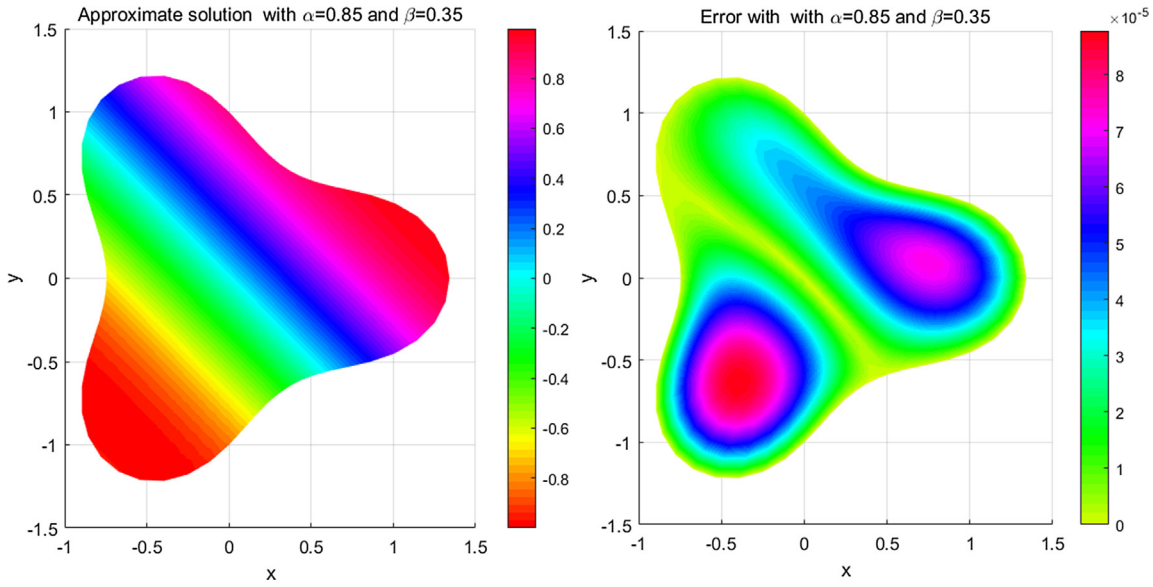

Fig. 10. The numerical solutions and the resulting errors at final time $T = 1$ on region Ω_4 of Example 2.

Table 11
Numerical orders of convergence in the time variable of the proposed method with $N = 441$ and $N_s = 79$ for Example 3.

δt	$\alpha = 0.65, \beta = 0.45, \gamma = 1/5$		$\alpha = 0.35, \beta = 0.95, \gamma = 1/10$	
	L_∞	$C_{\delta t}$	L_∞	$C_{\delta t}$
1/4	$6.4325e-02$	–	$8.5265e-02$	–
1/8	$2.5107e-02$	1.3573	$3.5791e-02$	1.2524
1/16	$9.7363e-03$	1.3966	$1.4830e-02$	1.2711
1/32	$3.6518e-03$	1.4148	$6.0150e-03$	1.3019
1/64	$1.3574e-03$	1.4278	$2.3965e-03$	1.3276
1/128	$4.9716e-04$	1.4491	$9.3132e-04$	1.3636

Example 3. Consider the following Gaussian pulse example

$$\frac{\partial u(x,y,t)}{\partial t} - \mathrm{D}_t^{1-\alpha}\Delta u(x,y,t) - \mathrm{D}_t^{1-\beta}\Delta u(\mathbf{x},t) = f(x,y,t), \qquad (x,y) \in \Omega, \qquad 0 < t \leqslant T.$$

All conditions and source term are deduced from the analytic solution $u(x,y,t) = t^{1+\alpha+\beta}\exp\left(\frac{-(x-0.5)^2-(y-0.5)^2}{\gamma}\right)$.

The new method is adopted for determining the numerical solution with various values of α, β and γ at final times T. Table 11 lists the L_∞ errors and the time convergence orders $C_{\delta t}$ of the proposed method for various values of α, β and γ at final time $T = 1$ on the square domain $[-2,2]^2$ including the uniform nodes. It can be seen that the obtained convergence rates tend to a limit close to $\mathcal{O}\left(\delta t^{1+\min\{\alpha,\beta\}}\right)$, which is in accordance with the theoretical convergence order. Fig. 11 depicts the approximate solutions and associated errors by choosing various values of $\gamma \in \{1/5, 1/10, 1/20\}$ on the square domain $[-2,2]^2$ having the uniform nodes with $\{\alpha = 0.55, \beta = 0.85\}$ $\delta t = 1/100, N = 441$ and $N_s = 87$ at $T = 1$.

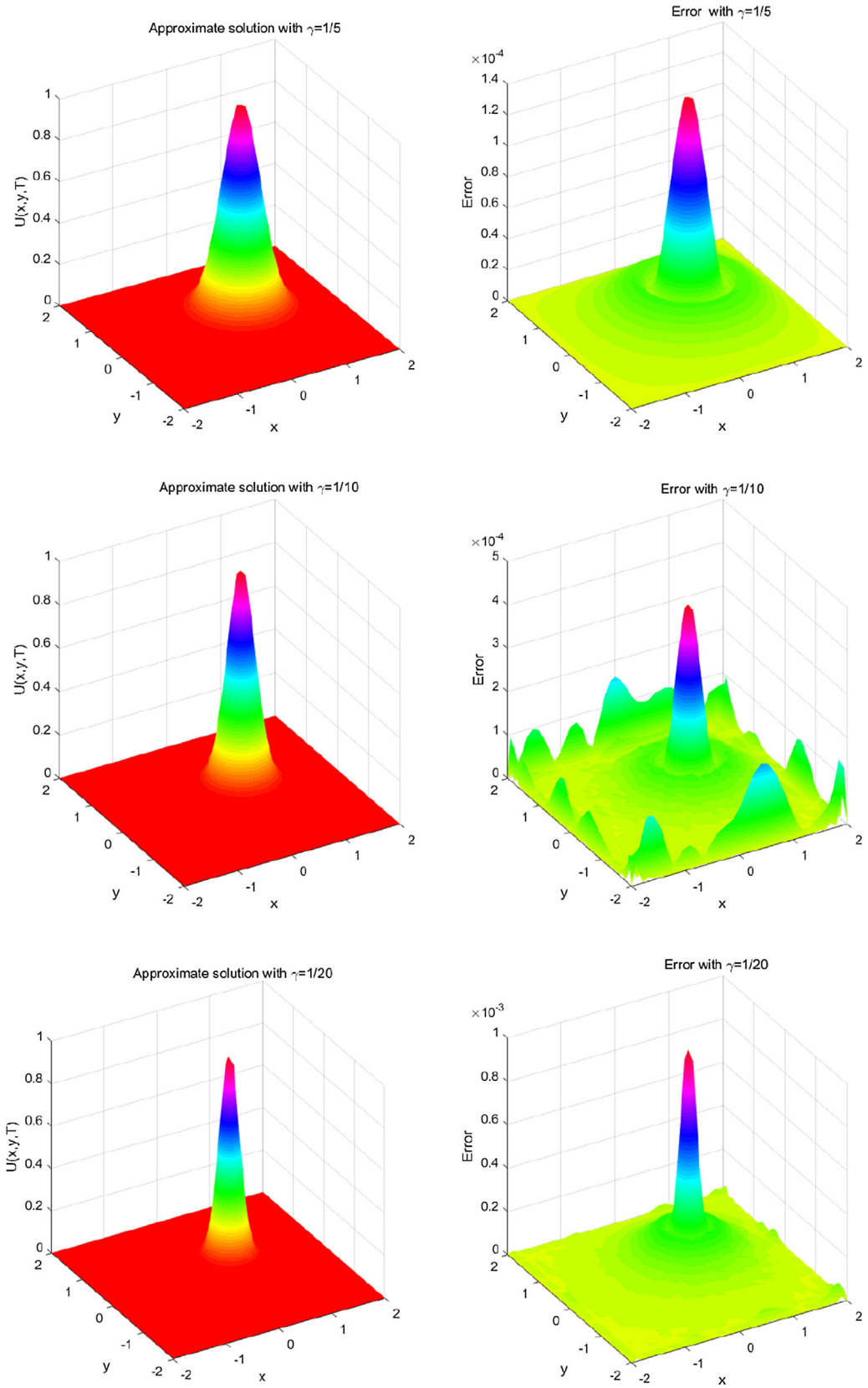

Fig. 11. Approximate solutions and errors on the square domain for $\gamma \in \{1/5, 1/10, 1/20\}$ with $\delta t = 1/100, N = 225$ on $[-2, 2]^2$ at $T = 1$ for Example 3.

Conclusion

Fractional diffusion models phenomena of anomalous diffusion in transport processes through complex and disordered systems with fractal media. This paper adopted a local hybrid kernel meshless strategy to solve the TFMDE. We observe in the published literature that some numerical algorithms have a high-order numerical accuracy on domains with simple shapes, but they are not applicable in the case of complex and irregular domains. On the other hand, some other techniques can be used on complex domains, but they exhibit in sufficient accuracy. Given these limitations, this paper presented a new local hybrid kernel meshless method. This approach not only provides adequate precision, but is also usable over complex domains with various node distributions. First, a finite difference scheme was employed to approximate the time direction. The unconditionally stability and convergence analysis of the semi-discrete approach were examined. Second, the local hybridization of Gaussian and cubic kernels method were used to discrete the spatial direction. Numerical simulations verified the good performance of the meshless algorithm on regular and irregular domains. The numerical results are compatible with the theoretical conclusions.

Declaration of Competing Interest

The authors declare no competing interests.

Compliance with ethics requirement

This paper does not include any studies with human or animal subjects.

Acknowledgements

The authors would like to thank the editors and three anonymous reviewers for their insightful comments and suggestions that greatly improved the quality of this paper.

References

[1] Oldham KB, Spanier J. The Fractional Calculus, vol. 111 of Mathematics in science and engineering; 1974.
[2] Podlubny I. Fractional differential equations: an introduction to fractional derivatives, fractional differential equations, to methods of their solution and some of their applications, Vol. 198. Elsevier; 1998.
[3] Uchaikin VV. Fractional derivatives for physicists and engineers, Vol. 2. Springer; 2013.
[4] Milici C, Drăgănescu G, Machado JT. Introduction to fractional differential equations, Vol. 25. Springer; 2019.
[5] Pinto C, Carvalho AR. Fractional dynamics of an infection model with time-varying drug exposure. J Comput Nonlinear Dyn 2018;13(9). Article 090904.
[6] Carvalho AR, Pinto CM, Tavares JN. Maintenance of the latent reservoir by pyroptosis and superinfection in a fractional order HIV transmission model. Int J Optim Control: Theories Appl (IJOCTA) 2019;9(3):69–75.
[7] Sweilam N, AL-Mekhlafi S, Albalawi A, Machado JT. Optimal control of variable-order fractional model for delay cancer treatments. Appl Math Model 2021;89:1557–74.
[8] Sweilam N, AL-Mekhlafi S, Baleanu D. Nonstandard finite difference method for solving complex-order fractional Burgers' equations. J Adv Res 2020;25:19–29.
[9] Tuan NH, Baleanu D, Thach TN, O'Regan D, Can NH. Final value problem for nonlinear time fractional reaction–diffusion equation with discrete data. J Comput Appl Math 2020;376:112883.
[10] Dubey VP, Kumar R, Kumar D, Khan I, Singh J. An efficient computational scheme for nonlinear time fractional systems of partial differential equations arising in physical sciences. Adv Diff Eqs 2020;2020(1):46.
[11] Luc NH, Huynh LN, Baleanu D, Can NH. Identifying the space source term problem for a generalization of the fractional diffusion equation with hyper-Bessel operator. Adv Diff Eqs 2020;2020(1):1–23.
[12] Dwivedi KD, Das S, Baleanu D. Numerical solution of nonlinear space–time fractional-order advection–reaction–diffusion equation. J Comput Nonlinear Dyn 2020;15(6):061005.
[13] Dehghan M, Manafian J, Saadatmandi A. Solving nonlinear fractional partial differential equations using the homotopy analysis method. Numer Methods Partial Diff Eqs: An Int J 2010;26(2):448–79.
[14] Dehghan M, Abbaszadeh M, Deng W. Fourth-order numerical method for the space–time tempered fractional diffusion-wave equation. Appl Math Lett 2017;73:120–7.
[15] Metzler R, Klafter J. Boundary value problems for fractional diffusion equations. Phys A 2000;278(1–2):107–25.
[16] Podlubny I. Geometric and physical interpretation of fractional integration and fractional differentiation, arXiv preprint math/0110241.
[17] Vlahos L, Isliker H, Kominis Y, Hizanidis K. Normal and anomalous diffusion: A tutorial, arXiv preprint arXiv:0805.0419.
[18] Tadjeran C, Meerschaert MM. A second-order accurate numerical method for the two-dimensional fractional diffusion equation. J Comput Phys 2007;220(2):813–23.
[19] Ciesielski M, Leszczynski J. Numerical simulations of anomalous diffusion, arXiv preprint math-ph/0309007.
[20] O'Shaughnessy B, Procaccia I. Diffusion on fractals. Phys Rev A 1985;32(5):3073.
[21] Chen W, Sun H, Zhang X, Korošak D. Anomalous diffusion modeling by fractal and fractional derivatives. Comput Math Appl 2010;59(5):1754–8.
[22] Paradisi P, Cesari R, Mainardi F, Tampieri F. The fractional Fick's law for non-local transport processes. Phys A 2001;293(1–2):130–42.
[23] Zhang H, Liu F, Anh V. Numerical approximation of Lévy-Feller diffusion equation and its probability interpretation. J Comput Appl Math 2007;206(2):1098–115.
[24] Płociniczak Ł. Analytical studies of a time-fractional porous medium equation. Derivation, approximation and applications. Commun Nonlinear Sci Numer Simul 2015;24(1–3):169–83.
[25] Thiel F, Flegel F, Sokolov IM. Disentangling sources of anomalous diffusion. Phys Rev Lett 2013;111(1):010601.
[26] Rozenbaum VM, Shapochkina IV. Analytical representation of the relations of inertial diffusion transport. JETP Lett 2015;102(4):248–53.
[27] Metzler R, Klafter J. The random walk's guide to anomalous diffusion: a fractional dynamics approach. Phys Rep 2000;339(1):1–77.
[28] Scalas E. Five years of continuous-time random walks in econophysics. In: The complex networks of economic interactions. Springer; 2006. p. 3–16.
[29] Liu Q, Liu F, Turner I, Anh V. Finite element approximation for a modified anomalous subdiffusion equation. Appl Math Model 2011;35(8):4103–16.
[30] Mohebbi A, Abbaszadeh M, Dehghan M. Solution of two-dimensional modified anomalous fractional sub-diffusion equation via radial basis functions (RBF) meshless method. Eng Anal Bound Elem 2014;38:72–82.
[31] Dehghan M, Abbaszadeh M, Mohebbi A. Legendre spectral element method for solving time fractional modified anomalous sub-diffusion equation. Appl Math Model 2016;40(5–6):3635–54.
[32] Wang T, Wang Y-M. A compact lod method and its extrapolation for two-dimensional modified anomalous fractional sub-diffusion equations. Comput Math Appl 2016;71(1):147–70.
[33] Li Y, Wang D. Improved efficient difference method for the modified anomalous sub-diffusion equation with a nonlinear source term. Int J Comput Math 2017;94(4):821–40.
[34] Shivanian E, Jafarabadi A. Time fractional modified anomalous sub-diffusion equation with a nonlinear source term through locally applied meshless radial point interpolation. Mod Phys Lett B 2018;32(22):1850251.
[35] Cao X, Cao X, Wen L. The implicit midpoint method for the modified anomalous sub-diffusion equation with a nonlinear source term. J Comput Appl Math 2017;318:199–210.
[36] Franke C, Schaback R. Convergence order estimates of meshless collocation methods using radial basis functions. Adv Comput Math 1998;8(4):381–99.
[37] Micchelli CA. Interpolation of scattered data: distance matrices and conditionally positive definite functions. In: Approximation theory and spline functions. Springer; 1984. p. 143–5.
[38] Madych W, Nelson S. Multivariate interpolation and conditionally positive definite functions. ii. Math Comput 1990;54(189):211–30.
[39] Hardy RL. Multiquadric equations of topography and other irregular surfaces. J Geophys Res 1971;76(8):1905–15.
[40] Kansa EJ. Multiquadrics-a scattered data approximation scheme with applications to computational fluid-dynamics-i surface approximations and partial derivative estimates. Comput Math Appl 1990;19(8–9):127–45.
[41] Kansa E, Hon Y. Circumventing the ill-conditioning problem with multiquadric radial basis functions: applications to elliptic partial differential equations. Comput Math Appl 2000;39(7–8):123–38.
[42] Tolstykh A, Shirobokov D. On using radial basis functions in a "finite difference mode with applications to elasticity problems. Comput Mech 2003;33(1):68–79.
[43] Abbaszadeh M, Dehghan M. Reduced order modeling of time-dependent incompressible Navier-Stokes equation with variable density based on a local radial basis functions-finite difference (LRBF-FD) technique and the POD/DEIM method. Comput Methods Appl Mech Eng 2020;364:112914.
[44] Dehghan M, Shafieeabyaneh N. Local radial basis function–finite-difference method to simulate some models in the nonlinear wave phenomena: regularized long-wave and extended Fisher-Kolmogorov equations. Eng Comput 2019:1–21. doi: https://doi.org/10.1007/s00366-019-00877-z.
[45] Dehghan M, Abbaszadeh M. The meshless local collocation method for solving multi-dimensional Cahn-hilliard, Swift-Hohenberg and phase field crystal equations. Eng Anal Bound Elem 2017;78:49–64.

[46] Avazzadeh Z, Nikan O, Machado JAT. Solitary wave solutions of the generalized Rosenau-KdV-RLW equation. Mathematics 2020;8(9):1601.
[47] Nikan O, Avazzadeh Z, Machado JT. Numerical investigation of fractional nonlinear sine-Gordon and Klein-gordon models arising in relativistic quantum mechanics. Eng Anal Bound Elem 2020;120:223–37.
[48] Nikan O, Machado J, Avazzadeh Z, Jafari H. Numerical evaluation of fractional Tricomi-type model arising from physical problems of gas dynamics. J Adv Res 2020;25:205–16.
[49] Nikan O, Machado JT, Golbabai A. Numerical solution of time-fractional fourth-order reaction-diffusion model arising in composite environments. Appl Math Model 2020;89:819–36.
[50] Zhuang P-H, Liu Q-X. Numerical method of Rayleigh-Stokes problem for heated generalized second grade fluid with fractional derivative. Appl Math Mech 2009;30(12):1533.
[51] Liu F, Zhuang P, Burrage K. Numerical methods and analysis for a class of fractional advection–dispersion models. Comput Math Appl 2012;64 (10):2990–3007.
[52] Lin Y, Li X, Xu C. Finite difference/spectral approximations for the fractional cable equation. Math Comput 2011;80(275):1369–96.
[53] Zhang N, Deng W, Wu Y. Finite difference/element method for a two-dimensional modified fractional diffusion equation. Adv Appl Math Mech 2012;4(4):496–518.
[54] Wendland H. Scattered data approximation, Vol. 17. Cambridge University Press; 2004.
[55] Buhmann MD. Radial basis functions: theory and implementations, Vol. 12. Cambridge University Press; 2003.
[56] Mishra PK, Nath SK, Sen MK, Fasshauer GE. Hybrid Gaussian-cubic radial basis functions for scattered data interpolation. Comput Geosci 2018;22 (5):1203–18.
[57] Mishra PK, Nath SK, Kosec G, Sen MK. An improved radial basis-pseudospectral method with hybrid Gaussian-cubic kernels. Eng Anal Bound Elem 2017;80:162–71.
[58] Mishra PK, Fasshauer GE, Sen MK, Ling L. A stabilized radial basis-finite difference (RBF-FD) method with hybrid kernels. Comput Math Appl 2019;77 (9):2354–68.
[59] Oruç Ö. A local hybrid kernel meshless method for numerical solutions of two-dimensional fractional cable equation in neuronal dynamics. Numer Methods Partial Diff Eqs 2020;36(6):1699–717.
[60] Kansa EJ. Multiquadrics-A scattered data approximation scheme with applications to computational fluid-dynamics-i surface approximations and partial derivative estimates. Comput Math Appl 1990;19(8–9):127–45.
[61] Kansa EJ. Multiquadrics-a scattered data approximation scheme with applications to computational fluid-dynamics-ii solutions to parabolic, hyperbolic and elliptic partial differential equations. Comput Math Appl 1990;19(8–9):147–61.
[62] Shu C, Ding H, Yeo K. Local radial basis function-based differential quadrature method and its application to solve two-dimensional incompressible Navier-Stokes equations. Comput Methods Appl Mech Eng 2003;192(7–8):941–54.
[63] Wright GB, Fornberg B. Scattered node compact finite difference-type formulas generated from radial basis functions. J Comput Phys 2006;212(1):99–123.
[64] Fasshauer GE. Meshfree Approximation Methods with Matlab:(With CD-ROM), Vol. 6, World Scientific Publishing Co Inc; 2007.
[65] Shechter G. Matlab package kd-tree; 2004.

Zakieh Avazzadeh is an Associate Professor at Xi'an Jiaotong-Liverpool University Suzhou, Jiangsu, China. She received her Ph.D. degree in Applied Mathematics from Yazd University in 2011. From 2012 to 2014, she was a postdoctoral fellowship at Hohai University. Her research areas are Numerical Approximation, Meshless Methods and Orthogonal Basis Functions. She is also interested in Fractional Calculus and Fractional Dynamical Systems.